BIOCHEMISTRY
including biophysical chemistry & molecular biology

Article

pubs.acs.org/biochemistry

Single Turnover of Substrate-Bound Ferric Cysteine Dioxygenase with Superoxide Anion: Enzymatic Reactivation, Product Formation, and a Transient Intermediate

Joshua A. Crawford, Wei Li, and Brad S. Pierce*

Department of Chemistry and Biochemistry, College of Sciences, The University of Texas at Arlington, Arlington, Texas 76019, United States

Supporting Information

ABSTRACT: Cysteine dioxygenase (CDO) is a non-heme mononuclear iron enzyme that catalyzes the O_2-dependent oxidation of L-cysteine (Cys) to produce cysteine sulfinic acid (CSA). In this study we demonstrate that the catalytic cycle of CDO can be "primed" by one electron through chemical oxidation to produce CDO with ferric iron in the active site (Fe^{III}-CDO, termed **2**). While catalytically inactive, the substrate-bound form of Fe^{III}-CDO (**2a**) is more amenable to interrogation by UV−vis and EPR spectroscopy than the 'as-isolated' Fe^{II}-CDO enzyme (**1**). Chemical-rescue experiments were performed in which superoxide ($O_2^{\bullet-}$) anions were introduced to **2a** to explore the possibility that a Fe^{III}-superoxide species represents the first intermediate within the catalytic pathway of CDO. In principle, $O_2^{\bullet-}$ can serve as a suitable acceptor for the remaining 3-electrons necessary for CSA formation and regeneration of the active Fe^{II}-CDO enzyme (**1**). Indeed, addition of $O_2^{\bullet-}$ to **2a** resulted in the rapid formation of a transient species (termed **3a**) observable at 565 nm by UV−vis spectroscopy. The subsequent decay of **3a** is kinetically matched to CSA formation. Moreover, a signal attributed to **3a** was also identified using parallel mode X-band EPR spectroscopy ($g \sim 11$). Spectroscopic simulations, observed temperature dependence, and the microwave power saturation behavior of **3a** are consistent with a ground state $S = 3$ from a ferromagnetically coupled ($J \sim -8$ cm^{-1}) high-spin ferric iron ($S_A = 5/2$) with a bound radical ($S_B = 1/2$), presumably $O_2^{\bullet-}$. Following treatment with $O_2^{\bullet-}$, the specific activity of recovered CDO increased to ∼60% relative to untreated enzyme.

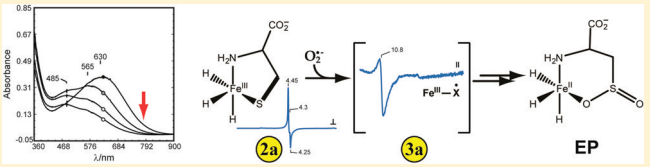

Cysteine dioxygenase (CDO) [EC 1.13.11.20] is a mononuclear non-heme iron enzyme that catalyzes the O_2-dependent oxidation of L-cysteine (Cys) to produce cysteine sulfinic acid (CSA).[1−4] This enzyme catalyzes the first committed step in the catabolic dissimilation of Cys to produce inorganic sulfate, pyruvate, hypotaurine, and taurine.[5] Intracellular Cys concentration is the limiting factor in glutathione (GSH) synthesis; therefore, the activity of CDO directly competes with cellular redox buffering under conditions of low Cys availability and oxidative stress. In response to such conditions, CDO is degraded by the ubiquitin−proteasome system in a cysteine-responsive manner.[6] Recently, the study of enzymes involved in mammalian sulfur-metabolism have been of considerable medical interest due to the observation that patients suffering from neurological disorders such as autism and Down syndrome have significantly lower plasma concentration of transsulfuration pathway and methionine cycle products [Cys, homocysteine (HCY), and GSH, and *S*-adenosylmethionine (SAM)].[7,8] In fact, imbalances in Cys metabolism have been identified in a variety of other neurological disorders as well (motor neuron, Parkinson's, and Alzheimer's disease).[9−11] These observations suggest a potential correlation between impaired sulfur-metabolism, oxidative stress, and neurodegenerative disease.[7]

CDO exhibits high specificity for L-cysteine, displaying little or no reactivity with D-cysteine, glutathione, L-cystine, or cysteamine. While results from steady-state kinetics of recombinant CDO are available, few direct mechanistic details are known.[10,12,13]

Multiple high-resolution crystal structures of mammalian CDO have been determined (pdb codes 2ATF, 2B5H, and 2IC1).[14−16] As illustrated in Figure 1A, the active site coordination of CDO is comprised of iron ligated by the N_ε-atoms of His86, His88, and His140, representing a new 3-His (3H) variant on the classic 2-His-1-carboxylate facial triad observed in mononuclear nonheme iron enzymes.[17] To date, only two enzymes with a 3H facial triad motif (CDO and diketone dioxygenase, Dke1) have been crystallographically[18] and spectroscopically characterized.[19,20] However, it has been proposed on the basis of sequence homology that the active site of cysteamine (2-aminoethanethiol) dioxygenase (ADO) also contains a 3H facial triad.[21]

Within 3.3 Å of the non-heme iron CDO active site is a covalently cross-linked cysteine−tyrosine pair (C93−Y157). An analogous post-transcriptional modification has been observed

Received: July 29, 2011
Revised: October 10, 2011
Published: October 12, 2011

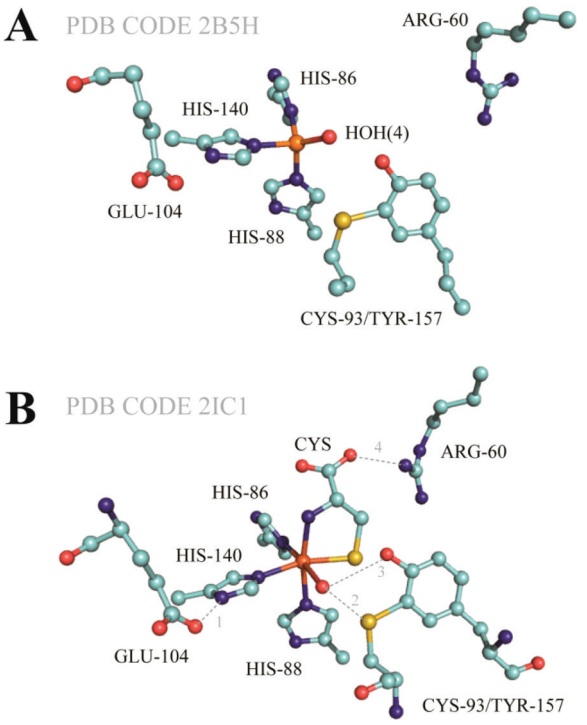

Figure 1. (A) 1.5 Å resolution crystal structure of the resting Fe^{II}-CDO enzyme (pdb code 2B5H).[15] (B) 2.7 Å resolution crystal structure of the substrate-bound CDO active site (pdb code 2IC1).[14] Selected distances indicated by 1, 2, 3, and 4 are 2.8, 2.6, 3.4, and 2.6 Å, respectively.

previously in only three other enzymes.[22−24] Since one of these enzymes is the copper radical enzyme, galactose oxidase (GO), it was initially proposed that a cysteine−tyrosine radical may also be involved in the oxidation of Cys.[14] However, mutations at C93 and Y157 lower, but do not abolish, enzymatic activity.[14,25] Moreover, the analogous C93 and Y157 residues are not conserved among putative bacterial CDO enzymes.[26] It has also been observed that addition of known radical scavengers such as hydroxyurea have no effect on steady-state kinetics of recombinant CDO.[27] On the basis of these observations, it is unlikely that the C93−Y157 pair of mammalian CDO is catalytically essential. Regardless, neither the mechanism of C93−Y157 formation nor its role in enzymatic catalysis is currently understood.

Prior to the addition of O_2, Cys coordinates to the mononuclear ferrous site of CDO in a bidentate fashion through a thiolate and neutral amine.[14,16,27] Presumably, the hydrogen bond between E104 and H140 results in a unique Cys amine binding site *trans* to H140.[27] Additional ligation of the Cys thiol group within the trigonal plane opposite H86 and H88 positions the carboxylate group of Cys favorably for charge stabilization by the R60 guanidinium group. This ternary interaction between Cys and the enzymatic active site shown in Figure 1B explains the high substrate specificity exhibited by CDO. A sixth coordination site would then be available for binding of molecular oxygen.

Within the 2-His-1-carboxylate family of non-heme iron containing oxidases and oxygenases, a general mechanism for catalysis has emerged based on extensive synthetic, mechanistic, spectroscopic, and crystallographic characterization.[28−30] Typically, the monoanionic active site contains a 5- or 6-coordinate ferrous iron with solvent molecules serving as the non-protein ligands. In the absence of substrate and/or cofactor, the reduced active site is unreactive toward O_2.[30] Similar behavior has also been observed for CDO. In experiments where nitric oxide (NO) was used as a surrogate for O_2 binding, CDO demonstrated an obligate-ordered binding of Cys prior to NO.[27]

Based on this 2-His-1-carboxylate model, and the limited mechanistic information available, at least two reasonable reaction pathways have been proposed for CDO (Figure 2), which ultimately lead to the production of L-cysteine sulfinic acid and a ferrous iron resting state for the enzyme. In the first step, binding of oxygen to the substrate-bound ferrous active site (**A**) would result in an internal electron transfer producing

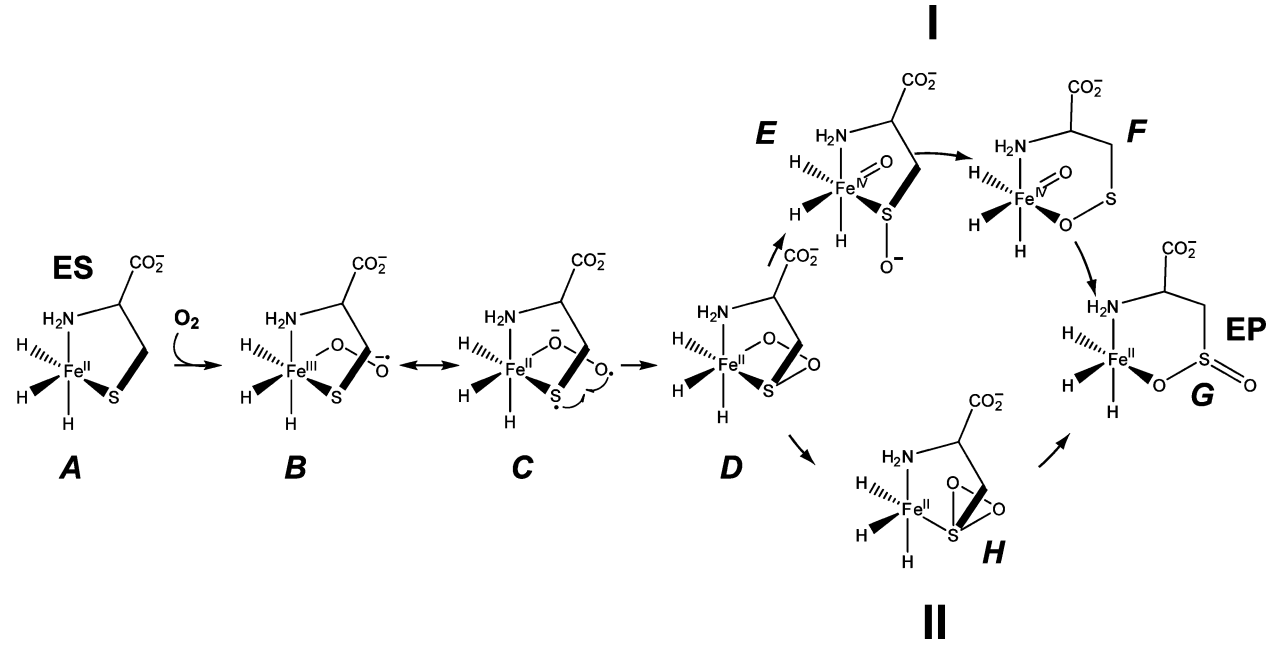

Figure 2. Proposed mechanistic pathways for CDO-catalyzed oxidation of Cys to produce CSA.[27,31−33,43]

dx.doi.org/10.1021/bi2011724|*Biochemistry* 2011, 50, 10241−10253

a short-lived ferric-superoxo [Fe^{III}-$O_2^{\bullet-}$] species (**B**). Resonance charge transfer between the ferric iron and the bound Cys thiolate could impart transient radical character on the S-atom (**C**), resulting in rapid recombination of bound superoxide and thiol radicals. The formation of the cyclic 4-membered Fe−O−O−S ring structure (**D**) has no precedent in 2-His-1-carboxylate enzymes; however, numerous reported DFT and QM/MM computations of CDO intermediates indicate that this structure is energetically favorable.[31−33] At this point, the reaction mechanism diverges to support the formation of two proposed intermediates. Shown in the upper pathway (**I**), heterolytic cleavage of the O−O bond would result in the formation of a transient Fe^{IV}-oxo species (**E**) such as those identified for a variety of O_2-activating 2-His-1-carboxylate oxygenase enzymes [taurine α-ketoglutarate (αKG)-dependent dioxygenase (TauD) and prolyl-4-hydroxylase (P4H)].[34−38] This model is supported by DFT and QM/MM computational studies; however, no experimental evidence for such an intermediate currently exists. On the basis of computational modeling, it has been proposed that rapid rearrangement of (**E**) to favor direct coordination of the cysteine sulfenate O-atom (**F**) directly precedes final Fe^{IV}-oxo rebound to generate a ferrous iron bound CSA (**G**).[31−33] Interestingly, the model proposed on the basis of DFT and QM/MM computations for the CSA-bound resting enzyme (**G**) suggests direct O-atom coordination of CSA. Typically, model complexes containing metal-bound sulfinates derived from oxidation of thiolate ligands are coordinated through the sulfinate S-atom.[39−41] Indeed, direct S-atom sulfinate coordination is also observed in the mononuclear Fe(III) active site of nitrile hydratase.[42] Another feature of this model currently debated is whether or not the neutral 3H ligand set of CDO is sufficiently π-donating to stabilize a Fe^{IV}−O intermediate. Moreover, the bidentate S/N-atom coordination observed for the Cys-bound active site would be less stabilizing for high valent iron−oxo intermediates as compared to α-ketoglutarate (αKG) coordination in αKG-dependent dioxygenase.

Recently, a putative ferrous iron-bound persulfenate intermediate was identified crystallographically within CDO. On this basis, an alternative mechanism for CSA formation has been proposed by Simmons et al.[43] An adaptation of this mechanism is shown in the lower pathway of Figure 2 (**II**). Starting from the neutral Fe−O−O−S cyclic persulfenate ring (**D**), nucleophilic attack of the proximal O-atom on the S-atom of the persulfenate would result in formation of a Cys-thiadioxirane ring (**H**). Subsequent heterolytic cleavage of the O−O bond would result in the formation of the CSA product and resting ferrous enzyme (**G**). In principle, direct nucleophilic attack of the Fe-bound thiolate on O_2 could bypass steps **B** through **D**, thus going directly from the substrate-bound enzyme (**A**) to the thiadioxirane (**G**). A similar reaction mechanism has been proposed in the O_2-dependent thiol-oxidation observed in nickel(II)−thiolate model complexes.[44,45] Given the absence of a high-valent Fe−oxo intermediate, this lower pathway is most comparable to the "substrate-activating" reaction mechanism proposed for Fe^{II}-containing homoprotocatechuate 2,3-dioxygenase (2,3-HPCD).[46]

A common feature for reaction mechanisms is the formation of a transient substrate-bound Fe^{III}-superoxo species (**B**). Indeed, ferric-superoxide intermediates have been proposed for several 2-His-1-carboxylate non-heme mononuclear iron enzymes including isopenicillin N synthase (IPNS), 1-aminocyclopropane-1-carboxylic acid oxidase (ACCO), and hydroxyethylphosphonate dioxygenase (HEPD).[47−49] However, to date, only one such example has been spectroscopically identified, (2,3-HPCD).[50] Interestingly, the catalytically active, Mn^{II}-substituted form of 2,3-HPCD also produces a transient Mn^{III}-superoxo species upon addition of oxygen to the substrate-bound enzyme.[51,52] Thus, it is possible that Fe^{III}-superoxo intermediate are a common mechanistic feature for both oxidase and oxygenase reactions.

The work presented here explores a chemical-rescue approach by which a putative substrate-bound Fe^{III}-superoxide species can be produced and spectroscopically characterized in CDO. A summary of the experiments performed is shown in Scheme 1. Briefly, samples of catalytically active Fe^{II}-containing

Scheme 1. Summary of Experiments

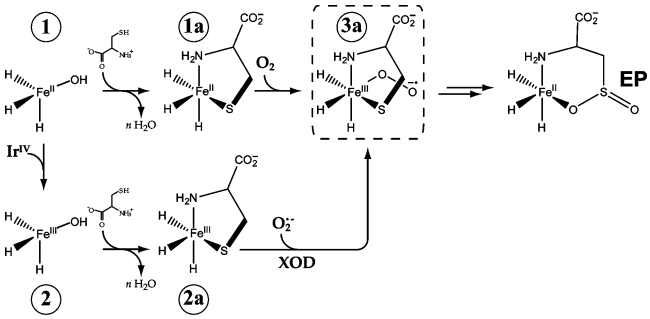

enzyme (**1**) were oxidized by treatment with potassium hexachloroiridate, K_2IrCl_6, to produce a catalytically inactive, Fe^{III}-containing enzyme (**2**). Addition of Cys to samples of **2** produced the substrate-bound Fe^{III}-CDO species (**2a**) previously characterized by UV−vis, CD/MCD, and resonance Raman spectroscopy.[53] Within samples of **2a**, aqueous superoxide anions were generated by xanthine oxidase-catalyzed univalent O_2-reduction. In theory, superoxide can act as a suitable oxidant to accept the remaining three electrons required for CSA formation and regenerate the catalytically active CDO species **1**. Following introduction of $O_2^{\bullet-}$, an unusually long-lived intermediate (**3a**) ($t_{1/2}$ ∼ 1.2 min) is observed by UV−vis and EPR spectroscopy. The decay of this intermediate is kinetically matched to CSA formation. Moreover, enzymatic activity of CDO is recovered upon treating **2a** with superoxide. To our knowledge, this is the first reported instance of superoxide-rescue for a non-heme iron enzyme. Freeze-quenched samples of **3a** were characterized by EPR spectroscopy, and spectroscopic simulations indicate that **3a** is best described as an antiferromagnetically coupled $S_A = 5/2$ with $S_B = 1/2$ resulting in a ground state $S = 3$. Thus, the observed spin state of CDO intermediate **3a** is consistent with the assignment of a substrate-bound Fe^{III}-superoxide intermediate species, analogous to the initial step (**B**) of the proposed reaction mechanism for CDO-catalyzed thiol-oxidation shown in Figure 2.

MATERIALS AND METHODS

Purification of CDO. Overexpression and purification of recombinant mouse CDO enzyme was performed with minor modifications to the procedure previously described.[27] In a typical purification, ∼30 g of *E. coli* BL21(DE3) cell paste was thawed in 100 mL of lysis buffer (25 mM HEPES, pH 8.0). To the resulting slurry, 10 mg of lysozyme and 2 mg each of RNase

and DNase (Sigma-Aldrich, St. Louis, MO) were added. The slurry was then mixed by hand on ice for 20 min prior to pulsed sonication for 10 min. Following sonication, the suspension was centrifuged for 1 h at 40000*g* at 4 °C to remove cell debris. The supernatant was diluted 1:1 with the lysis buffer and loaded onto a DEAE Sepharose anion exchange column pre-equilibrated in lysis buffer. The anion exchange column was washed with one column volume of wash buffer (25 mM HEPES, 30 mM NaCl, pH 8.0) prior to gradient elution from 50 to 350 mM NaCl. The fractions were pooled based on CDO activity as determined by TLC assay (described below) and the presence of the maltose binding protein−CDO fusion (MBP−CDO) observed by SDS PAGE. The pooled fractions were concentrated to approximately 5−10 mL using an Amicon stir cell equipped with an YM-30 ultrafiltration membrane. Tobacco etch virus protease (TEV) was used to cleave CDO from the fusion protein (4 h ambient temperature) in 50 mM HEPES, 100 mM NaCl, 0.3 mM tris(2-carboxyethyl)phosphine hydrochloride (TCEP), pH 7.5. A Sephacryl S-100 size exclusion column was used to separate MBP from CDO in 25 mM HEPES, 50 mM maltose, 150 mM NaCl, pH 7.5. The purified CDO enzyme was assayed for iron content as previously described, and protein content was determined by Bio-Rad protein assay. In a typical preparation, Fe-incorporation within CDO is approximately 50−60% relative to protein concentration. Since adventitious iron binding to CDO could potentially interfere with spectroscopic characterization, iron reconstitution was not attempted. Therefore, the concentrations reported for all experiments reflect the concentration of ferrous iron within samples of CDO. When normalized for Fe^{II} content, the Michaelis−Menten parameters (k_{cat} and K_M) determined for product formation were 2.2 s^{-1} and 3 mM, respectively ($V/K \sim 730\ M^{-1}\ s^{-1}$). These values are consistent with those previously reported for CDO.[27,53] Batches of CDO used in these experiments typically contain ∼80% C93−Y157 as determined by SDS PAGE densitometry. The freely available software ImageJ was used for analysis of SDS PAGE densitometry.

TLC CDO Activity Assay. Following column purification, fractions were selected based on qualitative CDO activity determination by thin-layer chromatography (TLC). From selected fractions a 50 μL aliquot was taken and placed in a 37 °C incubator. L-Cysteine was added to this solution for a final concentration of 10 mM. At 0, 15, and 30 min, 1 μL of the reaction was spotted onto a silica gel 60 F254 TLC plate (VWR) alongside 5 mM L-cysteine and cysteine sulfinic acid standards. After spotting the sample on the TLC plate a heat gun was used to completely dry the plate prior to elution for 20 min using a mobile phase of 20:20:60 (v/v) H_2O, acetic acid, and *n*-butanol, respectively. Following elution, the solvent front was marked and the plate was dried by a heat gun. The TLC plate was stained with ninhydrin (3 g of ninhydrin, 200 mL of ethanol, 6 mL of acetic acid) and developed by a heat gun.

HPLC CDO Activity Assay. The rate of cysteine sulfinic acid formation was determined by HPLC by a modified version of the method previously described.[27] Briefly, 1 μM CDO enzyme was allowed to react aerobically with L-cysteine for up to 30 min at 37 °C in 25 mM HEPES, 50 mM NaCl, pH 7.5. Samples were taken at selected time points for determination of L-cysteine and cysteinesulfinic acid concentration by reverse phase HPLC using 99.4:0.6 (v/v) water:methanol with 1% heptafluorobutyric acid, pH 2.0, as the mobile phase. Each sample aliquot was filtered by 0.22 μM cellulose acetate membrane (Corning, Spin-X) prior to analysis on HPLC. Injections (50 μL) were eluted at a flow rate of 1.0 mL/min on a Phenomenex Kinetex 2.6 μm C18 100 Å column (100 × 4.6 mm) and detected at 218 nm. HPLC samples were analyzed using a Dionex UltiMate 3000 HPLC equipped with a 3000 variable wavelength detector. The concentration of CSA produced in steady-state assays was determined by comparison to a 7-point standard curve (0.1−10 mM CSA) run in parallel with kinetic samples.

Anaerobic Work. All anaerobic samples were prepared in a glovebox (Coy Laboratory Products Inc., Grass City, MI) with the O_2 concentration maintained below 1 ppm. Solutions were degassed on a Schlenk line prior to transferring into the anaerobic chamber. Analytical grade argon was passed through a copper catalyst (Kontes, Vineland, NJ) to remove trace O_2 impurities and then sparged through distilled water to hydrate the gas.

K_2IrCl_6 Oxidation of Fe^{II}-CDO. Solutions of potassium hexachloroiridate [K_2IrCl_6] (15 mM) were prepared in aerobic buffer (25 mM HEPES, 50 mM NaCl, pH 8.0). In a typical reaction, a slight molar excess of hexachloroiridate (3 equiv per enzyme) was added to samples of CDO. This solution was allowed to equilibrate for 30 min at 4 °C prior to Sephadex G-25 gel filtration [$1.5D \times 15L$] to remove excess iridium species. Both Sephadex G-25 size exclusion and DEAE Sepharose anion exchange resins were found to be equally effective in removing residual iridium species from treated proteins samples. Following gel filtration, the iron content within samples of Fe^{III}-CDO was determined as described elsewhere. Enzymatic inactivation by potassium hexachloroiridate treatment was confirmed by HPLC and TLC assays as described above.

Addition of Superoxide to Substrate-Bound Fe^{III}-CDO. Xanthine oxidase (Sigma, St. Louis, MO) was used to generate superoxide anions by univalent reduction of oxygen using a modified version of the method described by Fridovich et al.[54−56] Briefly, a buffer containing 50 mM HEPES, 50 mM NaCl, 150 μM L-cysteine, 6 μM xanthine, pH 8.2 was sparged for 1 h with pure O_2 gas at 20 °C. CDO was added to this solution to obtain a final concentration 100 μM Fe^{III}-CDO within a quartz cuvette. Each reaction was initiated by spiking 0.4 units of xanthine oxidase into the cuvette using a Hamilton gastight syringe. Decay of the substrate-bound Fe^{III}-CDO was followed spectrophotometrically at 650 nm, and the amount of CSA produced in these reactions was determined by HPLC. Sample aliquots (200 μL) were taken directly from the cuvette at selected times (1−10 min). Each aliquot was immediately heat denatured at 95 °C and filtered by a spin-X centrifugal filter (Corning) to remove the precipitated protein. HPLC samples were prepared and analyzed as described above. LC-MS analysis of selected HPLC samples was performed as secondary confirmation of CSA product formation. The amount of superoxide produced by xanthine oxidase in the conditions described above was determined by monitoring the reduction of cytochrome *c* (Sigma, St. Louis, MO) by UV−vis spectroscopy (550 nm) according to published methods.[55,57] Catalase and superoxide dismutase (Sigma, St. Louis, MO) were added for control reactions to confirm the specificity of the cytochrome *c* assay for superoxide.

Spectroscopy. All UV−vis measurements were performed on an Agilent 8453 photo diode array spectrometer (Santa Clara, CA). Sample temperature was held constant by a 13 L circulating water bath and an Agilent thermostatable cell holder (89054A) with magnetic stirrer. All measurements were made

in ES Quartz cuvettes (NSG Precision Cells, Farmingdale, NY). X-band (9 GHz) EPR spectra were recorded on a Bruker (Billerica, MA) EMX Plus spectrometer equipped with a bimodal resonator (Bruker model 4116DM). Low-temperature measurements were made using an Oxford ESR900 cryostat and an Oxford ITC 503 temperature controller. A modulation frequency of 100 kHz was used for all EPR spectra. All experimental data used for spin quantitation were collected under nonsaturating conditions.

Analysis of the EPR spectra utilized the general spin Hamiltonian

$$\hat{H} = JS_A S_B + D\left(\hat{S}_Z{}^2 - \frac{S(S+1)}{3}\right) + E(\hat{S}_X{}^2 + \hat{S}_Y{}^2) + \beta BgS$$

where D and E are the axial and rhombic zero-field splitting (zfs) parameters, g is the g-tensor, and J is the Heisenberg-exchange constant.[58] EPR spectra were simulated and quantified using Spin Count (ver. 3.1.2), created by Professor M. P. Hendrich at Carnegie Mellon University. The simulations were generated with consideration of all intensity factors, both theoretical and experimental, to allow for determination of species concentration. The only unknown factor relating the spin concentration to signal intensity was an instrumental factor that is specific to the microwave detection system. However, this was determined by the spin standard, Cu(EDTA), prepared from a copper atomic absorption standard solution purchased from Sigma-Aldrich.

RESULTS

Production of Fe^{III}-CDO (2). As discussed in the Materials and Methods section, samples of resting Fe^{II}-CDO (termed CDO species **1**) were treated with a slight excess of potassium hexachloroiridate(IV) (E_m = +870 mV)[59−61] for 30 min on ice. Excess iridium species were removed by Sephadex G25 gel filtration. Following treatment of **1** with K_2IrCl_6, the catalytic activity of CDO is essentially zero. However, enzymatic activity is fully restored (~95% relative to as-isolated enzyme) upon reduction with hydroxylamine or sodium dithionite mediated by methyl viologen. This result indicates that K_2IrCl_6 oxidation of CDO is reversible and does not adversely affect the integrity of the enzyme. No evidence was obtained by either EPR or UV−vis spectroscopy to suggest the presence of adventitious iridium within treated samples of CDO.

Prior to the addition of substrate, the UV−vis spectrum of the Ir^{IV}-treated enzyme (termed **2**) is indistinguishable from the resting enzyme. However, as shown in Figure 3, addition of Cys produces an intense ligand to metal charge transfer (LMCT) band at 650 nm. This band is consistent with the oxidized substrate-bound enzyme (**2a**) which has been previously characterized by UV−vis, CD/MCD, resonance Raman spectroscopy, and supporting DFT calculations.[53] CDO species **2a** is very stable, showing only minor decay (<10%) in the observed absorbance at 650 nm over 30 min at ambient temperature, thus suggesting that Cys is not capable of rapidly reducing the ferric enzyme. On the basis of the aforementioned spectroscopic work, the active site geometry of **2a** is believed to approximate that of the active ferrous enzyme prior to the binding of O_2.

Deprotonation of the Cys ammonium and thiol groups is necessary for direct coordination of Cys to CDO species **2**.

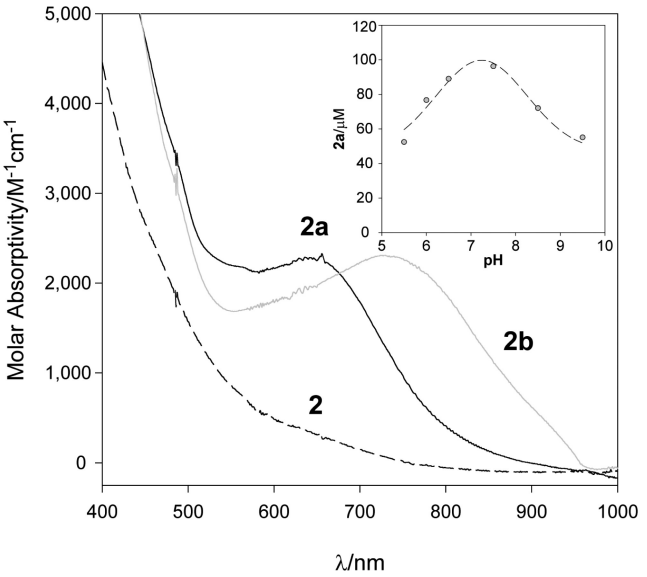

Figure 3. UV−vis spectrum of Fe^{III}-CDO (**2**) [dashed line], Cys-bound Fe^{III}-CDO (**2a**) [solid black line], and Sec-bound Fe^{III}-CDO (**2b**) [solid gray line] in 25 mM HEPES, 50 mM NaCl, pH 7.8. Inset: optimal pH for Cys binding to Fe^{III}-CDO (**2**) as observed by UV−vis spectroscopy.

Therefore, it is reasonable that the formation of **2a** would be pH-dependent. A pH profile was conducted to determine the optimal pH for the binding of Cys to **2**. In these experiments, 150 μM samples of **2** were prepared within an appropriate Good's buffer (100 mM) [MES (pK_a 6.1), HEPES (pK_a 7.5), and CHES (pK_a 9.3)] over a pH range of 5.5−9.5. To each sample, a substoichiometric amount of Cys (0.7 equiv per **2**) was added and allowed to equilibrate at 4 °C for 15 min. The amount of **2a** produced was measured spectrophotometrically at 650 nm. Additionally, aliquots of **2a** were prepared for analysis by EPR spectroscopy (discussed below). The extinction coefficient of **2a** was determined by dividing the recorded absorbance at 650 nm observed by UV−vis spectroscopy by the concentration of **2a** determined by EPR spin-quantitation. Using this approach, a more accurate determination of the **2a** extinction coefficient was obtained (ε_{650} = 2200 M^{-1} cm^{-1}). As indicated by Figure 3 (inset), CDO species **2** shows an optimal binding of Cys at pH 7.4 with ~95% of the total Cys added producing **2a**. No appreciable change in the extinction coefficient of **2a** was observed within the pH range of these experiments.

As shown in Figure 4A, the X-band EPR spectra of **2** exhibits an isotropic resonance at $g \sim 4.3$ and a much weaker resonance at $g \sim 8.3$ (spectrum *i*, top). The $g \sim 4.3$ feature originates from the middle doublet of a high-spin rhombic ($E/D \sim 1/3$) ferric iron (S = 5/2) center, whereas the $g \sim 8.3$ feature can be attributed to overlapping resonances within the lowest and highest lying doublets of the S = 5/2 spin system. Spin-quantitation of spectrum *i* accounts for ~95% of the total iron within the sample as determined spectrophotometrically. On the basis of this spectrum alone, it is difficult to determine if the observed ferric iron resides within the active site of CDO or is adventitiously bound to the protein. However, upon addition of a slight excess Cys (1.5 equiv per species **2**), spectrum *i* is completely converted to spectrum *ii* (bottom). The observed spectra (*ii*) show unusually sharp rhombic features at $g_{x,y,z}$ = 4.47, 4.36, and 4.27 as well as a set of weaker resonances at $g \sim$

dx.doi.org/10.1021/bi2011724|Biochemistry 2011, 50, 10241−10253

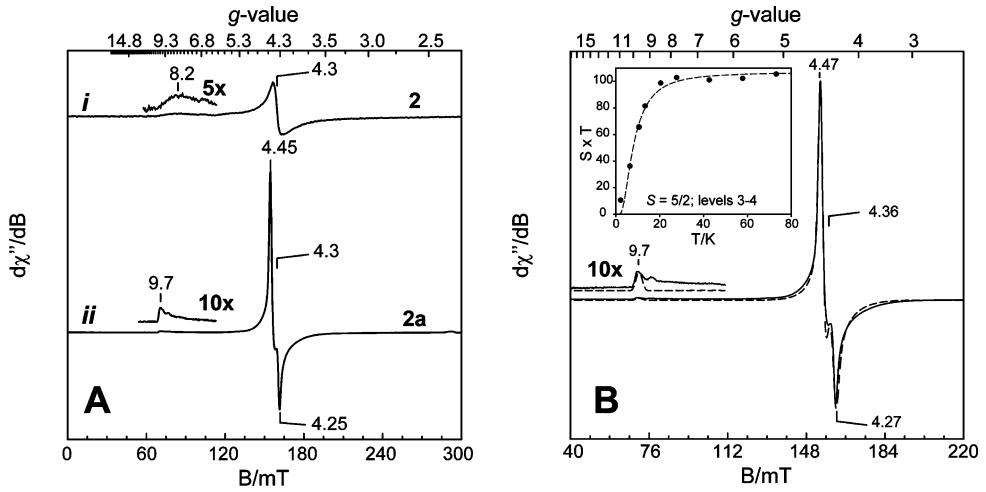

Figure 4. (A) 10 K X-band EPR spectra of CDO Fe^{III}-CDO (spectrum *i*, **2**) and Cys-bound Fe^{III}-CDO (spectrum *ii*, **2a**). (B) Quantitative EPR simulation (dashed line) overlaid on spectrum *ii* (solid line). Instrumental parameters: temperature, 10 K; microwave frequency, 9.62 GHz; microwave power, 2.0 mW; modulation amplitude, 1.0 mT. Simulation parameters: $S = 5/2$, $g_{x,y,z} = 2.081, 2.004, 1.976$; $|D| = 2.7\ cm^{-1}$; $\sigma_D = 0.02\ cm^{-1}$; $E/D = 0.31$; $\sigma_{E/D} = 0.06$; $\sigma_B = 0.9$ mT. The axial-zero field splitting term (D) for **2a** was determined by fitting the temperature normalized intensity of this signal (B, inset) to a Boltzmann population distribution for a three-level system.

9.7. The shift in the observed *g*-values for EPR spectra *ii* as compared to *i* can be attributed to the direct coordination of Cys to the iron site. The full conversion of spectrum *i* to *ii* upon addition of Cys indicates that all of the ferric iron observed by EPR spectroscopy must reside within the active site of CDO. On this basis, the signal observed for EPR spectra *ii* is assigned to the Cys-bound Fe^{III}-CDO (**2a**). A quantitative simulation (dashed line) for **2a** is overlaid on spectrum *ii* in Figure 4B. On the basis of this simulation, the concentration of **2a** was determined. The magnitude of the axial-zero field splitting term ($|D| = 2.7\ cm^{-1}$) for **2a** was determined by fitting the temperature normalized intensity of the $g_{ave} = 4.4$ signal (inset) to a Boltzmann population distribution for a three-level system. Table 1 lists all the relevant spectroscopic parameters for **2a**

Table 1. Spectroscopic Parameters for Substrate-Bound Oxidized CDO Species

parameter	(Fe^{III}-Cys) **2a**	(Fe^{III}-Sec) **2b**	(Fe^{III}-X•) **3a**
S	5/2	5/2	3
$g_{x,y,z}$	2.08, 2.00, 1.98	2.09, 2.00, 1.99	~2.00
$\|D\|$ (cm^{-1})	2.7	2.5	0.13
E/D	0.31	0.30	0.10
σ_D (cm^{-1})	0.02	0.02	<0.01
$\sigma_{E/D}$	0.06	0.05	0.03
J (cm^{-1})			-8 ± 3
σ_B (cm^{-1})	0.9	0.9	0.9
$P_{1/2}$ (mW), 10 K	90	195	25
λ (nm)	630	740	565
ε ($M^{-1}\ cm^{-1}$)	2200 ± 300	2300 ± 300	n/d

determined from EPR simulation. As expected, the direct S-atom coordination to the high-spin ferric iron site results in increased spin–orbit coupling of **2a** as compared to typical non-heme iron ferric centers. This is clearly reflected by the amount of microwave power required for half-saturation of the $S = 5/2$ EPR signal ($P_{1/2} = 90$ mW).

The binding of selenocysteine (Sec) to **2** was performed as an additional control to confirm that the Fe^{III}-CDO produced by treatment with K_2IrCl_6 is equivalent to the minor fraction of Fe^{III}-CDO previously characterized by resonance Raman and CD/MCD spectroscopy.[53] Shown in Figure 3 is the UV–vis spectrum of the Sec-bound Fe^{III}-CDO (termed **2b**) for comparison to **2a**. As previously reported, the Fe^{III}–Sec LMCT band for **2b** is significantly red-shifted relative to the Fe^{III}-Cys LMCT for **2a**. However, as indicated by Table 1, the EPR spectroscopic properties of **2b** showed only modest deviations from **2a**. The nearly identical zfs parameters of **2a** and **2b** indicate that the binding geometry of Cys and Sec to the active site of Fe^{III}-CDO are essentially identical. However, the half-power microwave saturation obtained for **2b** ($P_{1/2} = 195$ mW) is nearly twice that observed for **2a** at the same temperature (10 K). Collectively, these experiments clearly demonstrate that the Se-atom of Sec is directly coordinated to the ferric site of CDO. Moreover, these observations are consistent with the results obtained from previous published CD/MCD spectroscopic work.[53]

Addition of Superoxide Anion to Substrate-Bound Fe^{III}-CDO (2a). It has been previously demonstrated that xanthine oxidase (XO) can be utilized to catalyze the univalent reduction of O_2 to produce superoxide anion ($O_2^{\bullet-}$) within an aqueous solution.[54,55] Indeed, under appropriate conditions (basic conditions, substoichiometric xanthine concentration, and saturating O_2), XO is capable of converting a significant fraction of the oxygen present in solution into superoxide.[54] The most common method for detection of superoxide anions involves the spectrophotometric determination of cytochrome *c* reduction.[57] Using this procedure, the apparent second-order rate constant for superoxide-dependent cyt *c* reduction was determined to be ~1900 $M^{-1}\ s^{-1}$. This value is consistent with previously published results. As an additional control, superoxide formation was confirmed by EPR spectroscopy using the ($O_2^{\bullet-}$/•OH) spin-trap (DEPMPO) (Supporting Information).

In these experiments, XO was used to produce a steady-state concentration of superoxide in the presence of Cys-bound Fe^{III}-CDO (**2a**). For each reaction, a buffered solution (150 μM L-cysteine, 10 μM xanthine, pH 8.2) was sparged with pure O_2 for 1 h at 20 °C. Oxidized CDO (**2**) was added to the solution for a final **2a** concentration of 100 μM as confirmed by UV–vis

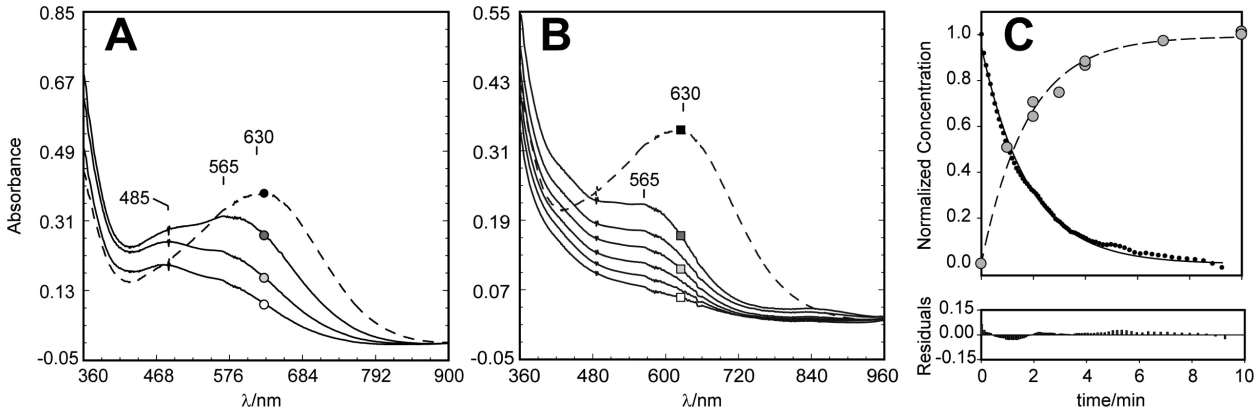

Figure 5. (A) Time-dependent change in the observed UV−vis spectrum of **2a** following addition of XO. The absorbance of **2a** before addition of XO is shown (A, B) by the dashed line. The circles (●, shaded ○, and ○) indicate spectra taken at 0.5, 1.0, and 2 s, respectively. (B) Time-dependent UV−vis spectra of **2a** upon addition of premixed (∼60 s) XO solution. The squares (■, shaded □, and □) indicate spectra taken at 0.5, 22, and 600 s, respectively. (C) Aliquots of reaction were taken at 0, 2, 3, 4, 7, and 10 min for CSA determination by HPLC. Data were fit to a single exponential to obtain an apparent first-order rate constant (k_{obs} = 0.6 min^{-1}). In multiple experiments (n = 5), 1.1 ± 0.2 mol equiv of CSA is produced per **2a** within 10 min.

spectroscopy. Production of superoxide was initiated by addition of 0.4 units XO under constant mixing at 20 °C.

As illustrated in Figure 5A, addition of XO to samples of **2a** in the presence of 6 μM xanthine and saturating O_2 resulted in formation of a new transient species (termed **3a**) with observable features at 485 and 565 nm. Complete loss of **2a** was observed within 5 s following addition of XO. Alternatively, the subsequent decay of **3a** was significantly slower. Given the competition between XO-dependent superoxide formation and the apparent consumption of superoxide by **2a**, the observed kinetics for this reaction are complicated. To simplify interpretation, the XO solution was premixed with xanthine and O_2 and allowed to react for 60 s prior to mixing with **2a**. This preincubation step allows superoxide to build up to a steady-state concentration prior to addition of **2a**, thus forcing the reaction into an apparent first-order regime. Other than the order of addition, all reagent concentrations remain constant. As illustrated in Figure 5B, incorporation of a 60 s premixing step simplifies the observed kinetics to an apparent first-order reaction in which only the decay of **3a** is observed. The decay of **3a** observed by UV−vis spectroscopy (black circles) can be reasonably fit assuming a single-exponential decay (k_{obs} = 0.6 min^{-1}). Given the relatively slow rate of **3a** decay, aliquots of this reaction were pulled at selected time points (1−10 min) for heat inactivation at 95 °C and analysis by HPLC. The determination of CSA formation was performed as described within the Materials and Methods section. For clarity, the scale for the ordinate is normalized for simultaneous comparison of UV−vis and HPLC results (Figure 5C). In these experiments, CSA formation (gray circles) is observed concomitant with the decay of **3a** (black circles). Selected reaction samples were analyzed by LC-MS for independent confirmation of correct product (CSA) formation.

To confirm that the CSA produced is not the direct product of Cys oxidation by $O_2^{\bullet-}$, control XO reactions were prepared containing excess Cys, but lacking **2**. However, no detectable amounts of CSA were observed within the time scale of these experiments (10 min). Moreover, addition of excess superoxide dismutase (SOD, 5 units) or known ($O_2^{\bullet-}$ and $^{\bullet}OH$) trapping reagents (DEPMPO, 10 mM) to XO reactions completely abolishes formation of the **3a** intermediate and CSA. Addition of catalase (5 units) to XO reactions appeared to decrease the rate of CSA formation slightly (∼13%); however, it has been previously demonstrated that, in addition to H_2O_2, catalase also reacts readily with superoxide anions.[62−64] Therefore, as an additional control, H_2O_2 (200 μM) was directly added to samples of **2a** to determine if it is (in part) responsible for the formation of CSA. However, no detectable amounts of CSA or **3a** were observed in these reactions. On the basis of these results, it can be reasonably concluded that only superoxide is reacting with **2a** to produce the physiologically relevant product (CSA) and the observed **3a** intermediate.

As illustrated in the superoxide-rescue pathway shown in Scheme 1, the formation of CSA by addition of $O_2^{\bullet-}$ to **2a** should also return CDO to its catalytically active state (**1**, Fe^{II}-CDO). Thus, the catalytic activity of CDO should be recovered following treatment with XO. Indeed, samples collected after 10 min treatment with XO showed 60% specific activity as compared to the as-isolated enzyme.

Superoxide can act as a mild reductant in aqueous solutions [$E(O_2/O_2^{\bullet-})$ = −0.16 V vs NHE].[65,66] Therefore, one possible explanation for the reactivation of CDO and subsequent product formation is that $O_2^{\bullet-}$ reduces **2a** to produce **1a** and 1 mol equiv of O_2. Rapid rebound of **1a** with the resulting O_2 would then initiate product formation via the native CDO reaction pathway. To explore this possibility, CDO species **2** was exposed to superoxide in the absence of substrate as described above for **2a**. Following treatment for 15 min, the reaction was quenched by addition of SOD and catalase (5 units each). Cys was then added to samples, and the amount of **2a** produced was determined by UV−vis spectroscopy. Therefore, any reduction of **2** by $O_2^{\bullet-}$ would result in decreased **2a** formation; however, no discernible decrease in the amount of **2a** produced was observed relative to untreated enzyme. Moreover, $O_2^{\bullet-}$ treated **2** remains catalytically inactive. Taken together, these results indicate that superoxide is not capable of reducing the oxidized enzyme.

EPR Spectroscopy of Putative Substrate-Bound Fe^{III}-Superoxo CDO (3a). Given the slow decay of **3a** observed spectrophotometrically, EPR samples could be produced by hand-mixing reagents and freezing in liquid N_2 at selected time points. Samples were frozen over ∼30 s to avoid breaking the quartz EPR tube during expansion of the freezing solution. Therefore, times specified refer to the time each sample was

placed into the liquid N_2. The preparation of EPR samples was carried out as described for the above UV−vis experiments with the exception that the final **2a** concentration (before addition of XO) was increased to 160 μM. As observed by UV−vis experiments, the binding of superoxide to **2a** appears to be quite rapid. In samples frozen ∼40 s after hand-mixing **2a** with XO, only trace amounts of **2a** could be observed in transverse mode ($B_1 \perp B$) EPR (data not shown). Spin-quantization reveals only ∼10 μM **2a** corresponding to ∼4% of the total iron in the sample. However, as shown in Figure 6A, a new signal can be observed at $g \sim 11$ (10 K, solid line) when the microwave field polarization is applied parallel to the static magnetic field ($B_1 \| B$). This signal exhibits inhomogeneous saturation behavior with a $P_{1/2}$ of 25 mW at 10 K. The observed spectra for **3a** is consistent with a transition within a "non-Kramers" doublet from an integer-spin paramagnetic center.

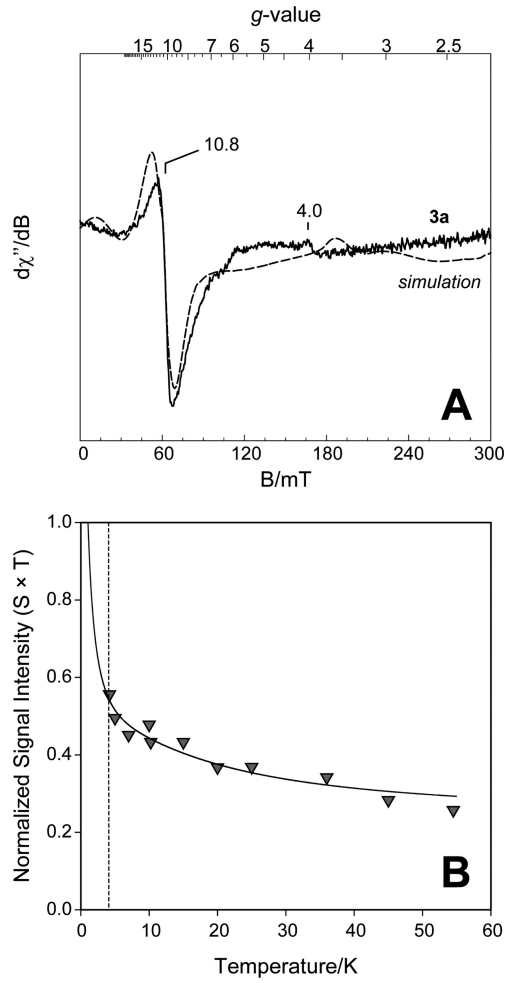

Figure 6. (A) Parallel mode X-band EPR spectra of **3a** produced following addition of XO to **2a**. A simulation (dashed line) for species **3a** is overlaid on the collected spectra (solid line). Instrumental parameters: temperature, 4.8 K; microwave frequency, 9.38 GHz; microwave power, 0.63 mW; modulation amplitude, 1.0 mT. Simulation parameters: $S = 3$, $g_{x,y,z} = 2.00$; $|D| = 0.13$ cm^{-1}; $\sigma_D = 0.007$ cm^{-1}; $E/D = 0.10$; $\sigma_{E/D} = 0.03$; $\sigma_B = 0.9$ mT. The concentration of **3a** determined by EPR simulation was ∼50 μM (∼30% of the total Fe-containing CDO). (B) Curie law normalized signal intensity (S × T) of **3a** as a function of temperature. The magnitude of the exchange coupling ($J = -8 \pm 3$ cm^{-1}; $H = JS_AS_B$) was determined by fitting the normalized signal intensity to the theoretical Boltzmann population (solid line) for a $S = 3$ multiplet. The dashed-vertical line designates the lowest temperature limit of the cryostat.

As previously mentioned, treatment of CDO with K_2IrCl_6 results in stoichiometric conversion of all Fe^{II} into Fe^{III}. Furthermore, neither superoxide nor Cys is capable of reducing Fe^{III}-CDO within the time scale of these experiments. Therefore, it is unlikely that this signal can be attributed to a high spin ferrous species ($S = 2$) spectroscopically distinct from the resting enzyme. It can also be argued qualitatively that the increased spin−orbit coupling from a (d^6) ferrous iron would significantly increase the electronic relaxation rates. However, at 10 K the $P_{1/2}$ value obtained for **3a** is relatively close in magnitude to the substrate-bound Fe^{III}-CDO species (25 vs 90 mW, respectively). For comparison, microwave power saturation data collected for synthetic 4-coordinate Fe(II) complexes exhibit significantly greater $P_{1/2}$ values (490 mW) on the same instrumentation with equivalent temperature, modulation amplitude, scan rate, and time constant (Figure S3).[67] On the basis of these observations, it is argued henceforth that the likely Fe-oxidation state of **3a** is +III.

On the basis of simple electron count, a Fe^{III}-superoxo species would be the expected product for this reaction. Antiferromagnetic (AF, $J > 0$) or ferromagnetic exchange (F, $J < 0$) coupling of a high-spin ferric iron ($S_A = 5/2$) and a superoxide anion ($S_B = 1/2$) would result in a ground $S = 2$ or $S = 3$ spin state, respectively. The observed resonance for this intermediate species lies between the expected g-values for an idealized $S = 2$ ($g \sim 8$) or $S = 3$ ($g \sim 12$) species. Therefore, EPR spectroscopic simulations for F ($S = 3$) and AF ($S = 2$) configurations of **3a** were performed. These calculations employ least-squares analysis of spectra data to allow variation of spectroscopic terms (g-values, D, and E/D) and a distribution in the zero-field splitting terms ($\sigma_{E/D}$, and σ_D). As indicated by Figure 6A (dashed line) the spectrum of **3a** could be reasonably fit for the F configuration with the spectroscopic parameters given in Table 1. As expected for a d^5 ion, the g-values obtained by simulation show little deviation from the free electron g value ($g_e = 2.0023$). Simulations were also attempted assuming AF exchange; however a reasonable match to the observed **3a** spectra could not be obtained without invoking unreasonably high g-anisotropy ($\Delta g \sim 0.37$) for the Fe site. Moreover, the concentration predicted by the AF simulation was exceedingly low as compared to the F simulation (∼50 μM). Given the half-life of **2a** observed by UV−vis spectroscopy ($t_{1/2} \sim 70$ s), the concentration of **3a** predicted by the F simulation (50 μM) is more consistent with the expected intermediate concentration when quenched at 40 s.

As indicated by the gray triangles in Figure 6B, the temperature normalized signal intensity of **3a** is most intense at 4.2 K and decreases gradually with increasing temperature. This observation suggests that the $g \sim 11$ signal likely originates from either the ground- or a very low-lying doublet. As shown by the solid line in Figure 6B, the temperature-dependent behavior of **3a** can be well fit assuming ferromagnetic exchange coupling of S_A and S_B ($J = -8$ cm^{-1}) with a small, axial zero-field splitting ($|D| \sim 0.13$ cm^{-1}). This is in good agreement with the simulation for **3a** shown in Figure 6A. As indicated by the theoretical fits to the temperature-dependent signal intensity of **3a**, the exchange interaction (J) is significantly larger than the axial zero-field splitting term (D) for both of the proposed F configuration. In this strong-exchange limit ($J/D \gg 1$), the spin system can be treated as an isolated $S = 3$ multiplet.

DISCUSSION

Oxidation of CDO Active Site. Previous spectroscopic work on Fe^{III}-CDO experiments relied on the presence of trace impurities of the catalytically inactive ferric enzyme.[53] However, batch to batch, the concentration of Fe^{III}-CDO is highly variable and often does not exceed 5% relative to the catalytically active ferrous enzyme. For this reason, potassium hexachloroiridate(IV) was used to chemically oxidize resting Fe^{II}-CDO (**1**) to produce the oxidized Fe^{III}-CDO (**2**). This reagent has been frequently employed in aqueous systems to oxidize various enzymes.[61,68] Both enzymatic activity assays and spectroscopic (UV−vis/EPR) results confirm near full conversion of **1** to **2** is obtained under mild conditions by treatment with a slight molar excess of K_2IrCl_6 (3 equiv relative to the Fe-containing enzyme). Moreover, since essentially full activity of CDO is restored upon chemical reduction, Ir-oxidation of CDO occurs reversibly and without any discernible damage to the protein.

EPR spectroscopy of the Cys- (**2a**) and Sec-bound Fe^{III}-CDO (**2b**) indicates that both species exhibit near identical axial zero-field splitting (D) and rhombicity (E/D). This result is in good agreement with the spectroscopic characterization of these species by CD/MCD spectroscopy.[53] Moreover, the doubling of the half-power saturation behavior ($P_{1/2}$) of **2b** (195 mW) relative to **2a** (90 mW) and the red-shifted LMCT of **2b** relative to **2a** observed by UV−vis spectroscopy confirms direct ferric-iron coordination of the Se and S-atom of Sec and Cys, respectively. Interestingly, both of these observations are in contrast to the reported EXAFS data for the substrate-bound resting enzyme.[69] Although the binding of Sec and Cys to the active site of CDO is geometrically equivalent, it should be noted that only Cys serves as a competent substrate for CDO.[53] By all activity assays (TLC, HPLC), no indication of CDO-catalyzed Sec oxidation could be observed. It can be argued that this can be attributed to the rapid oxidation of Sec directly by O_2 to produce L-selenocystine and H_2O_2.

Given the direct coordination of the deprotonated thiolate of Cys ($pK_a \sim 8.3$) to the CDO active-site iron, it is not surprising that the pH optimum for Cys-binding to **2** is strongly pH-dependent. The observed optimum (pH ∼ 7.5) for the formation of **2a** likely reflects the pK_a of the Cys-thiol group when coordinated to the Fe^{III}-active site. This value is close to the optimal pH for enzymatic activity reported by Chai et al. (pH 7.5) but is significantly higher than reported by Simmons et al. (pH 6.1).[10,12] Surprisingly, there is a wide range of optimal pH values reported for CDO (6.1−9.0) in the literature.[10,12,70,71] For batches of CDO described here, the pH-dependent steady-state rate of CSA formation agrees reasonably well with the observed pH optimum demonstrated for Cys-binding to the Fe^{III}-CDO (pH 8.0 and 7.5, respectively).

Putative Ferric-Superoxide Intermediate (3a) of CDO. In heme-containing enzymes, a variety of ferric-superoxide intermediates have been crystallographically and spectroscopically characterized.[72−74] However, few examples of such intermediates have been reported for non-heme iron enzymes.[50,75] The EPR spectroscopic parameters determined for **3a** are in good agreement with the Fe^{III}-superoxo species (**Int-1**) reported for 2,3-HPCD with a few notable exceptions. First of all, the observed line width of **3a** is broader than for **Int-1** in 2,3-HPCD. While several factors contribute to line broadening in parallel mode EPR spectra, the most likely explanation for this difference is increased spin−orbit coupling due to the direct coordination of the Cys S-atom. The EPR signal for the **3a** intermediate in CDO is well fit assuming ferromagnetically coupling of a high-spin Fe(III) ion ($S_A = 5/2$) with a radical, presumably $O_2^{\bullet-}$ ($S_B = 1/2$). Both the magnitude of the axial zero field-splitting term (D) and isotropic g-values observed for **3a** are consistent with a d^5 ferric ion. Moreover, the small axial zero field splitting ($|D| \sim 0.13$ cm^{-1}) is in good agreement with the D value reported for the nonheme iron Fe^{III}-superoxo species identified in 2,3-HPCD.[50] The magnitude of the spin exchange (J) is also comparable with the value reported for **Int-1** and suggests direct coordination of the paramagnetic centers. However, in contrast to the **Int-1** intermediate of 2,3-HPCD, **3a** exhibits ferromagnetic exchange ($J = -8$ cm^{-1}) coupling, giving rise to a ground state $S = 3$ multiplet. Alternatively, the exchange coupling for **Int-1** is antiferromagnetic ($J = +6$ cm^{-1}), resulting in a ground state $S = 2$ manifold. While the reason for this deviation is not yet clear, it can be speculated that this likely reflects a difference in the coordination geometry of the putative Fe^{III}-superoxo species in **3a** as compared to **Int-1** in 2,3-HPCD.

Mechanistic Implications. The experiments performed here demonstrate a chemical-rescue of the catalytically inactive substrate-bound Fe^{III}-CDO (**2a**) by treatment with superoxide ($O_2^{\bullet-}$). In many respects, the well-known peroxide-shunt pathway exhibited by both heme and non-heme monoxygenase enzymes can, to some extent, be thought of as a chemical-rescue for such enzymes lacking an electron-transport system. However, while chemical-rescue experiments have been performed on a variety of non-heme iron enzymes,[76−78] to our knowledge, superoxide has not been previously utilized as a chemical trigger to study the activity of non-heme mononuclear iron activities. In contrast to the peroxide-shunt pathway, superoxide-rescue experiments do not produce steady-state catalysis. Instead, only a single turnover of the substrate-bound Fe^{III}-CDO and recovery of active Fe^{II}-CDO enzyme is observed.

One striking feature regarding the work presented here is the relatively long lifetime and high accumulation of the **3a** intermediate upon triggering with superoxide. The formation of **3a** following initiation of XO-dependent $O_2^{\bullet-}$ generation is very rapid, exhibiting full conversion of **2a** within 5 s. Therefore, the binding of $O_2^{\bullet-}$ to **2a** does not appear to be rate-limiting in UV−vis reactions. Interestingly, while the rate of **3a** decay and product formation ($k_{obs} \sim 0.6$ min^{-1}) are kinetically matched, this rate is nearly 200-fold slower than the steady-state rate of native CDO catalysis ($k_{cat} \sim 2.2$ s^{-1}). Since chemical reduction of **2a** yields active enzyme with catalytic efficiency (V/K) equivalent to untreated enzyme, oxidation of CDO by hexachloroiridate does not cause any irreversible damage to CDO. Therefore, the unusual stability of the **3a** intermediate suggests an inherent difference in the local environment of the iron-active site of **2a** relative to the untreated ferrous enzyme (**1a**). For example, a protein conformation change or a difference in the protonation state of a nearby residue. One argument for the unusually long lifetime exhibited by this putative Fe^{III}-superoxide species can be made on the basis of the crystal structure for the putative persulfenate-bound enzyme shown in Figure 7.[43] In this work it was observed that the Y157 hydroxyl group of CDO is at a favorable distance to form a hydrogen bond with the proximal O-atom of the putative persulfenate intermediate. In theory, this interaction could stabilize the bound superoxide anion, thus

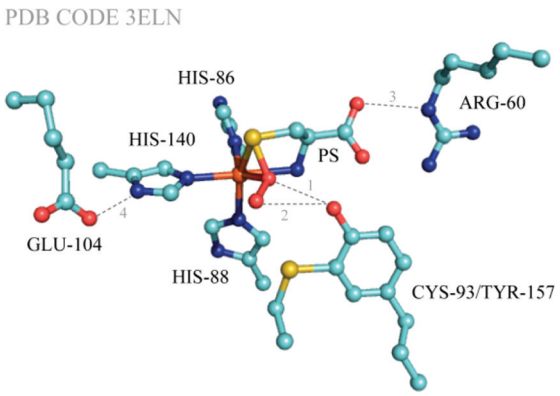

Figure 7. 1.4 Å resolution crystal structure of the putative Fe^{II}-bound Cys-persulfenate within the active site of CDO (pdb code 3ELN).[43] Selected distances indicated by 1, 2, 3, and 4 are 2.8, 3.2, 2.9, and 2.7 Å, respectively.

slowing its rate of attack on the Fe-bound Cys substrate. Several examples of stabilizing hydrogen bonding interactions to Fe^{III}-superoxo and Fe^{III}-peroxo species have been reported for both heme-containing and non-heme iron metalloproteins.[72,79−82]

Alternatively, the reaction pathway taken during native catalysis may be entirely divergent than that observed during superoxide-rescue experiments. If, for example, native catalysis in CDO follows a substrate-activating mechanism analogous to the Fe^{III}-dependent catechol dioxygenase, direct nucleophilic attack by the Fe-bound Cys-thiolate on molecular oxygen would precede CSA formation. The resulting thiadioxirane intermediate (Figure 2H) would bypass formation of a Fe^{III}-superoxide species entirely. Indeed, an analogous mechanism has been postulated for the "dioxygenase-like" behavior observed in 4-coordiante Ni(II)−thiolate complexes upon exposure to O_2.[44,45] However, this model is inconsistent with the observation that the substrate-bound resting enzyme readily binds nitric oxide to produce an unusual $\{FeNO\}^7$ ($S = 1/2$) species.[27] The direct coordination of NO to the enzyme−substrate CDO complex implies that O_2 would also favor direct coordination to the Fe site as opposed to the S-atom of the bound Cys-thiolate. Regardless, without additional experimental information it is not immediately clear how the native and superoxide-rescue pathways deviate mechanistically. It should also be noted that, up to this point, it has been assumed that the $S_B = 1/2$ site in **3a** is attributed to a superoxide anion. However, other possibilities cannot be excluded without supporting spectroscopic confirmation. Additional characterization of **3a** using resonance Raman and Mössbauer spectroscopy is planned in order to unambiguously assign intermediate **3a**.

In summary, the UV−vis and EPR spectroscopic characterization of **3a** provides a critical first glance at an intermediate species kinetically matched with product formation. While it is not clear if this transient species is produced within the native catalytic cycle of CDO, it offers a point of comparison to intermediates observed in other non-heme mononuclear iron enzymes. Given the similar electronic structure for **3a** in CDO and **Int-1** in 2,3-HPCD, it is tempting to speculate that CDO follows a similar mechanistic pathway as 2,3-HPCD, in which a Fe^{III}-superoxo intermediate facilitates substrate oxidation instead of a high-valent $Fe^{IV}(O)$ intermediate as indicated by the upper pathway (I) of Figure 2.

■ ASSOCIATED CONTENT

Ⓢ Supporting Information

The cyt *c* assay conditions used to measure the rate of superoxide produced by uncoupled xanthine oxidase catalysis (Figure S1); EPR spectra and assay conditions for DEPMPO-trapped superoxide (Figure S2); determination of the power-saturation behavior for **2a**, **2b**, and **3a** (Figure S3). This material is available free of charge via the Internet at http://pubs.acs.org.

■ AUTHOR INFORMATION

Corresponding Author

*Phone: (817) 272-9066. Fax: (817) 272-3808. E-mail: bspierce@uta.edu.

Funding

This work was supported by start-up funds provided by The University of Texas at Arlington, Department of Chemistry and Biochemistry.

■ ACKNOWLEDGMENTS

The authors thank the UTA Center for Nanostructured Materials for the use of EPR instrumentation. LC-MS data were collected with the assistance of Professor K. Schug, Department of Chemistry and Biochemistry (UTA). We also thank Professor M. P. Hendrich (Carnegie Mellon University) for providing the EPR analysis and simulation software (SpinCount) and for useful conversations.

■ ABBREVIATIONS

CDO, cysteine dioxygenase; SOD, superoxide dismutase; Cat, catalase; XO, xanthine oxidase; Cys, L-cysteine; Sec, selenocysteine; CSA, cysteine sulfinic acid; HPLC, high performance liquid chromatography; EPR, electron paramagnetic resonance; DEPMPO, 5-(diethoxyphosphoryl)-5-methyl-1-pyrroline *N*-oxide.

■ REFERENCES

(1) Stipanuk, M. H. (2004) Sulfur Amino Acid Metabolism: Pathways for Production and Removal of Homocysteine and Cysteine. *Annu. Rev. Nutr. 24*, 539−577.

(2) Ewetz, L., and Sorbo, B. (1966) Characteristics of the Cysteinesulfinate-Forming Enzyme System in Rat Liver. *Biochim. Biophys. Acta 128*, 296−305.

(3) Sorbo, B., and Ewetz, L. (1965) The Enzymatic Oxidation of Cysteine to Cysteinesulfinate in Rat Liver. *Biochem. Biophys. Res. Commun. 18*, 359−363.

(4) Lombardini, J. B., Singer, T. P., and Boyer, P. D. (1969) Cysteine Oxygenase. *J. Biol. Chem. 244*, 1172−1175.

(5) Stipanuk, M., Simmons, C., Andrew Karplus, P., and Dominy, J. (2010) Thiol dioxygenases: unique families of cupin proteins. *Amino Acids*, 1−12.

(6) Stipanuk, M. H., Hirschberger, L. L., Londono, M. P., Cresenzi, C. L., and Yu, A. F. (2004) The ubiquitin-proteasome system is responsible for cysteine-responsive regulation of cysteine dioxygenase concentration in liver. *Am. J. Physiol. Endocrinol. Metab. 286*, E439−E448.

(7) Deth, R., Muratore, C., Benzecry, J., Power-Charnitsky, V.-A., and Waly, M. (2008) How environmental and genetic factors combine to cause autism: A redox/methylation hypothesis. *NeuroToxicology 29*, 190−201.

(8) James, S. J., Cutler, P., Melnyk, S., Jernigan, S., Janak, L., Gaylor, D. W., and Neubrander, J. A. (2004) Metabolic biomarkers of increased oxidative stress and impaired methylation capacity in children with autism. *Am. J. Clin. Nutr. 80*, 1611−1617.

(9) Gordon, C., Emery, P., Bradley, H., and Waring, H. (1992) Abnormal sulfur oxidation in systemic lupus erythematosus. *Lancett 229*, 25−26.

(10) Simmons, C. R., Hirschberger, L. L., Machi, M. S., and Stipanuk, M. H. (2006) Expression, purification, and kinetic characterization of recombinant rat cysteine dioxygenase, a non-heme metalloenzyme necessary for regulation of cellular cysteine. *Protein Expr. Purif. 47*, 74−81.

(11) Heafield, M. T., Fearn, S., Steventon, G. B., Waring, R. H., Williams, A. C., and Sturman, S. G. (1990) Plasma cysteine and sulfate levels in patients with motor neurone, Parkinson's and Alzheimer's disease. *Neurosci. Lett. 110*, 216−220.

(12) Chai, S. C., Jerkins, A. A., Banik, J. J., Shalev, I., Pinkham, J. L., Uden, P. C., and Maroney, M. J. (2005) Heterlogous Expression, Purification, and Characterization of Recombinant Rat Cysteine Dioxygenase. *J. Biol. Chem. 280*, 9865−9869.

(13) Bagley, P. J., Hirschberger, L. L., and Stipanuk, M. H. (1995) Evaluation and Modification of an Assay Procedure for Cysteine Dioxygenase Activity: HPLC Method for Measurement of Cysteine Sulfinate and Demonstration of Physiological Relevance of Cysteine Dioxygenase Activity in Cysteine Catabolism. *Anal. Biochem. 227*, 40−48.

(14) Ye, S., Wu, X. a., Wei, L., Tang, D., Sun, P., Bartlam, M., and Rao, Z. (2007) An Insight into the Mechanism of Human Cysteine Dioxygenase: Key Roles of the Thioether-Bonded Tyrosine-Cysteine Cofactor. *J. Biol. Chem. 282*, 3391−3402.

(15) Simmons, C. R., Liu, Q., Huang, Q., Hao, Q., Begley, T. P., Karplus, P. A., and Stipanuk, M. H. (2006) Crystal Structure of Mammalian Cysteine Dioxygenase. *J. Biol. Chem. 281*, 18723−18733.

(16) McCoy, J. G., Bailey, L. J., Bitto, E., Bingman, C. A., Aceti, D. J., Fox, B. G., and Phillips, G. N. Jr. (2006) Structure and mechanism of mouse cysteine dioxygenase. *Proc. Natl. Acad. Sci. U. S. A. 103*, 3084−3089.

(17) Straganz, G. D., and Nidetzky, B. (2006) Variations of the 2-His-1-carboxylate Theme in Mononuclear Non-Heme Fe(II) Enzymes. *ChemBioChem 7*, 1536−1548.

(18) Unpublished crystal structure, RCSB Protein Data Bank ID (3BAL).

(19) Diebold, A. R., Neidig, M. L., Moran, G. R., Straganz, G. D., and Solomon, E. I. (2010) The Three-His Triad in Dke1: Comparisons to the Classical Facial Triad. *Biochemistry 49*, 6945−6952.

(20) Straganz, G. D., Diebold, A. R., Egger, S., Nidetzky, B., and Solomon, E. I. (2010) Kinetic and CD/MCD Spectroscopic Studies of the Atypical, Three-His-Ligated, Non-Heme Fe^{2+} Center in Diketone Dioxygenase: The Role of Hydrophilic Outer Shell Residues in Catalysis. *Biochemistry 49*, 996−1004.

(21) Dominy, J. E., Simmons, C. R., Hirschberger, L. L., Hwang, J., Coloso, R. M., and Stipanuk, M. H. (2007) Discovery and Characterization of a Second Mammalian Thiol Dioxygenase, Cysteamine Dioxygenase. *J. Biol. Chem. 282*, 25189−25198.

(22) Ito, N., Phillips, S. E. V., Stevens, C., Ogel, Z. B., McPherson, M. J., Keen, J. N., Yadav, K. D. S., and Knowles, P. F. (1991) Novel thioether bond revealed by a 1.7 Å crystal structure of galactose oxidase. *Nature 350*, 87−90.

(23) Schnell, R., Sandalova, T., Hellman, U., Lindqvist, Y., and Schneider, G. (2005) Siroheme- and $[Fe_4$-$S_4]$-dependent NirA from *Mycobacterium tuberculosis* Is a Sulfite Reductase with a Covalent Cys-Tyr Bond in the Active Site. *J. Biol. Chem. 280*, 27319−27328.

(24) Whittaker, J. W. (2003) Free Radical Catalysis by Galactose Oxidase. *Chem. Rev. 103*, 2347−2363.

(25) Dominy, J. E. Jr., Hwang, J., Guo, S., Hirschberger, L. L., Zhang, S., and Stipanuk, M. H. (2008) Synthesis of Amino Acid Cofactor in Cysteine Dioxygenase Is Regulated by Substrate and Represents a Novel Post-translational Regulation of Activity. *J. Biol. Chem. 283*, 12188−12201.

(26) Dominy, J. E. Jr., Simmons, C. R., Karplus, P. A., Gehring, A. M., and Stipanuk, M. H. (2006) Identification and Characterization of Bacterial Cysteine Dioxygenases: a New Route of Cysteine Degradation for Eubacteria. *J. Bacteriol. 188*, 5561−5569.

(27) Pierce, B. S., Gardner, J. D., Bailey, L. J., Brunold, T. C., and Fox, B. G. (2007) Characterization of the Nitrosyl Adduct of Substrate-Bound Mouse Cysteine Dioxygenase by Electron Paramagnetic Resonance: Electronic Structure of the Active Site and Mechanistic Implications. *Biochemistry 46*, 8569−8578.

(28) Solomon, E. I., Decker, A., and Lehnert, N. (2003) Non-heme iron enzymes: contrasts to heme catalysis. *Proc. Natl. Acad. Sci. U. S. A. 100*, 3589−3594.

(29) Solomon, E. I., Brunold, T. C., Davis, M. I., Kemsley, J. N., Lee, S.-K., Lehnert, N., Neese, F., Skulan, A. J., Yang, Y.-S., and Zhou, J. (2000) Geometric and Electronic Structure/Function Correlations in Non-Heme Iron Enzymes. *Chem. Rev. 100*, 235−349.

(30) Costas, M., Mehn, M. P., Jensen, M. P., and Que, L. J. (2004) Dioxygen Activation at Mononuclear Nonheme Iron Active Sites: Enzymes, Models, and Intermediates. *Chem. Rev. 104*, 939−986.

(31) Kumar, D., Thiel, W., and de Visser, S. P. (2011) Theoretical Study on the Mechanism of the Oxygen Activation Process in Cysteine Dioxygenase Enzymes. *J. Am. Chem. Soc. 133*, 3869−3882.

(32) de Visser, S. P., and Straganz, G. D. (2009) Why Do Cysteine Dioxygenase Enzymes Contain a 3-His Ligand Motif Rather than a 2His/1Asp Motif Like Most Nonheme Dioxygenases? *J. Phys. Chem. A 113*, 1835−1846.

(33) Aluri, S., and de Visser, S. P. (2007) The Mechanism of Cysteine Oxygenation by Cysteine Dioxygenase Enzymes. *J. Am. Chem. Soc. 129*, 14846−14847.

(34) Price, J. C., Barr, E. W., Tirupati, B., Bollinger, J. M., and Krebs, C. (2003) The First Direct Characterization of a High-Valent Iron Intermediate in the Reaction of an α-Ketoglutarate-Dependent Dioxygenase: A High-Spin Fe(IV) Complex in Taurine/α-Ketoglutarate Dioxygenase (TauD) from *Escherichia coli*. *Biochemistry 42*, 7497−7508.

(35) Hoffart, L. M., Barr, E. W., Guyer, R. B., Bollinger, J. M., and Krebs, C. (2006) Direct spectroscopic detection of a C-H-cleaving high-spin Fe(IV) complex in a prolyl-4-hydroxylase. *Proc. Natl. Acad. Sci. U. S. A. 103*, 14738−14743.

(36) Galonic Fujimori, D., Barr, E. W., Matthews, M. L., Koch, G. M., Yonce, J. R., Walsh, C. T., Bollinger, J. M., Krebs, C., and Riggs-Gelasco, P. J. (2007) Spectroscopic Evidence for a High-Spin Br-Fe(IV)-Oxo Intermediate in the α-Ketoglutarate-Dependent Halogenase CytC3 from *Streptomyces*. *J. Am. Chem. Soc. 129*, 13408−13409.

(37) Lange, S. J., Miyake, H., and Que, L. (1999) Evidence for a Nonheme Fe(IV)O Species in the Intramolecular Hydroxylation of a Phenyl Moiety. *J. Am. Chem. Soc. 121*, 6330−6331.

(38) Lim, M. H., Rohde, J.-U., Stubna, A., Bukowski, M. R., Costas, M., Ho, R. Y. N., Münck, E., Nam, W., and Que, L. (2003) An Fe(IV)O complex of a tetradentate tripodal nonheme ligand. *Proc. Natl. Acad. Sci. U. S. A. 100*, 3665−3670.

(39) Tyler, L. A., Noveron, J. C., Olmstead, M. M., and Mascharak, P. K. (1999) Oxidation of Metal-Bound Thiolato Sulfur Centers in Fe(III) and Co(III) Complexes with Carboxamido Nitrogens and Thiolato Sulfurs as Donors: Relevance to the Active Sites of Nitrile Hydratases. *Inorg. Chem. 38*, 616−617.

(40) Kung, I., Schweitzer, D., Shearer, J., Taylor, W. D., Jackson, H. L., Lovell, S., and Kovacs, J. A. (2000) How Do Oxidized Thiolate Ligands Affect the Electronic and Reactivity Properties of a Nitrile Hydratase Model Compound? *J. Am. Chem. Soc. 122*, 8299−8300.

(41) Buonomo, R. M., Font, I., Maguire, M. J., Reibenspies, J. H., Tuntulani, T., and Darensbourg, M. Y. (1995) Study of Sulfinate and Sulfenate Complexes Derived from the Oxygenation of Thiolate Sulfur in [1,5-Bis(2-mercapto-2-methylpropyl)-1,5-diazacyclooctanato(2-)]-nickel(II). *J. Am. Chem. Soc. 117*, 963−973.

(42) Dey, A., Chow, M., Taniguchi, K., Lugo-Mas, P., Davin, S., Maeda, M., Kovacs, J. A., Odaka, M., Hodgson, K. O., Hedman, B., and Solomon, E. I. (2005) Sulfur K-Edge XAS and DFT Calculations on Nitrile Hydratase: Geometric and Electronic Structure of the Non-heme Iron Active Site. *J. Am. Chem. Soc. 128*, 533−541.

(43) Simmons, C. R., Krishnamoorthy, K., Granett, S. L., Schuller, D. J., Dominy, J. E., Begley, T. P., Stipanuk, M. H., and Karplus, P. A.

(2008) A Putative Fe^{2+}-Bound Persulfenate Intermediate in Cysteine Dioxygenase. *Biochemistry 47*, 11390−11392.
(44) Maroney, M. J., Choudhury, S. B., Bryngelson, P. A., Mirza, S. A., and Sherrod, M. J. (1996) Theoretical Study of the Oxidation of Nickel Thiolate Complexes by O_2. *Inorg. Chem. 35*, 1073−1076.
(45) Mirza, S. A., Pressler, M. A., Kumar, M., Day, R. O., and Maroney, M. J. (1993) Oxidation of nickel thiolate ligands by dioxygen. *Inorg. Chem. 32*, 977−987.
(46) Kovaleva, E. G., and Lipscomb, J. D. (2007) Crystal Structures of Fe^{2+} Dioxygenase Superoxo, Alkylperoxo, and Bound Product Intermediates. *Science 316*, 453−457.
(47) Rocklin, A. M., Tierney, D. L., Kofman, V., Brunhuber, N. M. W., Hoffman, B. M., Christoffersen, R. E., Reich, N. O., Lipscomb, J. D., and Que, L. (1999) Role of the nonheme Fe(II) center in the biosynthesis of the plant hormone ethylene. *Proc. Natl. Acad. Sci. U. S. A. 96*, 7905−7909.
(48) Brown, C. D., Neidig, M. L., Neibergall, M. B., Lipscomb, J. D., and Solomon, E. I. (2007) VTVH-MCD and DFT Studies of Thiolate Bonding to $\{FeNO\}^7/\{FeO2\}^8$ Complexes of Isopenicillin N Synthase: Substrate Determination of Oxidase versus Oxygenase Activity in Nonheme Fe Enzymes. *J. Am. Chem. Soc. 129*, 7427−7438.
(49) Hirao, H., and Morokuma, K. (2010) Ferric Superoxide and Ferric Hydroxide Are Used in the Catalytic Mechanism of Hydroxyethylphosphonate Dioxygenase: A Density Functional Theory Investigation. *J. Am. Chem. Soc. 132*, 17901−17909.
(50) Mbughuni, M. M., Chakrabarti, M., Hayden, J. A., Bominaar, E. L., Hendrich, M. P., Münck, E., and Lipscomb, J. D. (2010) Trapping and spectroscopic characterization of an Fe^{III}-superoxo intermediate from a nonheme mononuclear iron-containing enzyme. *Proc. Natl. Acad. Sci. U. S. A. 107*, 16788−16793.
(51) Emerson, J. P., Kovaleva, E. G., Farquhar, E. R., Lipscomb, J. D., and Que, L. (2008) Swapping metals in Fe- and Mn-dependent dioxygenases: Evidence for oxygen activation without a change in metal redox state. *Proc. Natl. Acad. Sci. U. S. A. 105*, 7347−7352.
(52) Gunderson, W. A., Zatsman, A. I., Emerson, J. P., Farquhar, E. R., Que, L., Lipscomb, J. D., and Hendrich, M. P. (2008) Electron Paramagnetic Resonance Detection of Intermediates in the Enzymatic Cycle of an Extradiol Dioxygenase. *J. Am. Chem. Soc. 130*, 14465−14467.
(53) Gardner, J. D., Pierce, B. S., Fox, B. G., and Brunold, T. C. (2010) Spectroscopic and Computational Characterization of Substrate-Bound Mouse Cysteine Dioxygenase: Nature of the Ferrous and Ferric Cysteine Adducts and Mechanistic Implications. *Biochemistry 49*, 6033−6041.
(54) Fridovich, I. (1970) Quantitative Aspects of the Production of Superoxide Anion Radical by Milk Xanthine Oxidase. *J. Biol. Chem. 245*, 4053−4057.
(55) McCord, J. M., and Fridovich, I. (1968) The Reduction of Cytochrome c by Milk Xanthine Oxidase. *J. Biol. Chem. 243*, 5753−5760.
(56) McCord, J. M., and Fridovich, I. (1969) Superoxide Dismutase. *J. Biol. Chem. 244*, 6049−6055.
(57) Crack, J. C., Green, J., Cheesman, M. R., Le Brun, N. E., and Thomson, A. J. (2007) Superoxide-mediated amplification of the oxygen-induced switch from [4Fe-4S] to [2Fe-2S] clusters in the transcriptional regulator FNR. *Proc. Natl. Acad. Sci. U. S. A. 104*, 2092−2097.
(58) Abragam, A., and Bleaney, B. (1970) *Electron Paramagnetic Resonance of Transition Ions* (International Series of Monographs on Physics).
(59) Kwiatkowski, L. D., Adelman, M., Pennelly, R., and Kosman, D. J. (1981) Kinetic mechanism of the Cu(II) enzyme galactose oxidase. *J. Inorg. Biochem. 14*, 209−222.
(60) Niviére, V., Asso, M., Weill, C. O., Lombard, M., Guigliarelli, B., Favaudon, V., and Houée-Levin, C. (2003) Superoxide Reductase from *Desulfoarculus baarsii*:Identification of Protonation Steps in the Enzymatic Mechanism. *Biochemistry 43*, 808−818.
(61) Whittaker, M. M., Kersten, P. J., Cullen, D., and Whittaker, J. W. (1999) Identification of Catalytic Residues in Glyoxal Oxidase by Targeted Mutagenesis. *J. Biol. Chem. 274*, 36226−36232.
(62) Ghiladi, R. A., Medzihradszky, K. F., Rusnak, F. M., and Ortiz de Montellano, P. R. (2005) Correlation between Isoniazid Resistance and Superoxide Reactivity in *Mycobacterium tuberculosis* KatG. *J. Am. Chem. Soc. 127*, 13428−13442.
(63) Kono, Y., and Fridovich, I. (1982) Superoxide radical inhibits catalase. *J. Biol. Chem. 257*, 5751−5754.
(64) Shimizu, N., Kobayashi, K., and Hayashi, K. (1984) The reaction of superoxide radical with catalase. Mechanism of the inhibition of catalase by superoxide radical. *J. Biol. Chem. 259*, 4414−4418.
(65) Sawyer, D. T., and Valentine, J. S. (1981) How super is superoxide? *Acc. Chem. Res. 14*, 393−400.
(66) Wood, P. M. (1987) The two redox potentials for oxygen reduction to superoxide. *Trends Biochem. Sci. 12*, 250−251.
(67) Granum, D. M., Riedel, P. J., Crawford, J. A., Mahle, T. K., Wyss, C. M., Begej, A. K., Arulsamy, N., Pierce, B. S., and Mehn, M. P. (2011) Synthesis and Characterization of Sterically Encumbered β-Ketoiminate Complexes of Iron(II) and Zinc(II). *Dalton Trans. 40*, 5881−5890.
(68) Clay, M. D., Emerson, J. P., Coulter, E. D., Kurtz, D. M., and Johnson, M. K. (2003) Spectroscopic characterization of the $[Fe(His)_4(Cys)]$ site in 2Fe-superoxide reductase from *Desulfovibrio vulgaris*. *J. Biol. Inorg. Chem. 8*, 671−682.
(69) Chai, S. C., Bruyere, J. R., and Maroney, M. J. (2006) Probes of the Catalytic Site of Cysteine Dioxygenase. *J. Biol. Chem. 281*, 15774−15779.
(70) Yamaguchi, K., Hosokawa, Y., Kohashi, N., Kori, Y., Sakakibara, S., and Ueda, I. (1978) Rat Liver Cysteine Dioxygenase (Cysteine Oxidase). *J. Biochem. 83*, 479−491.
(71) Sakakibara, S., Yamaguchi, K., Hosokawa, Y., Kohashi, N., Ueda, I., and Sakamoto, Y. (1976) Purification and some properties of rat liver cysteine oxidase (cysteine dioxygenase). *Biochim. Biophys. Acta 422*, 273−279.
(72) Denisov, I. G., Mak, P. J., Makris, T. M., Sligar, S. G., and Kincaid, J. R. (2008) Resonance Raman Characterization of the Peroxo and Hydroperoxo Intermediates in Cytochrome P450. *J. Phys. Chem. A 112*, 13172−13179.
(73) Galinato, M. G. I., Spolitak, T., Ballou, D. P., and Lehnert, N. (2010) Elucidating the Role of the Proximal Cysteine Hydrogen-Bonding Network in Ferric Cytochrome P450cam and Corresponding Mutants Using Magnetic Circular Dichroism Spectroscopy. *Biochemistry 50*, 1053−1069.
(74) Hirotsu, S., Chu, G. C., Unno, M., Lee, D.-S., Yoshida, T., Park, S.-Y., Shiro, Y., and Ikeda-Saito, M. (2004) The Crystal Structures of the Ferric and Ferrous Forms of the Heme Complex of HmuO, a Heme Oxygenase of *Corynebacterium diphtheriae*. *J. Biol. Chem. 279*, 11937−11947.
(75) Xing, G., Diao, Y., Hoffart, L. M., Barr, E. W., Prabhu, K. S., Arner, R. J., Reddy, C. C., Krebs, C., and Bollinger, J. M. (2006) Evidence for C-H cleavage by an iron-superoxide complex in the glycol cleavage reaction catalyzed by myo-inositol oxygenase. *Proc. Natl. Acad. Sci. U. S. A. 103*, 6130−6135.
(76) Saleh, L., Krebs, C., Ley, B. A., Naik, S., Huynh, B. H., and Bollinger, J. M. (2004) Use of a Chemical Trigger for Electron Transfer to Characterize a Precursor to Cluster X in Assembly of the Iron-Radical Cofactor of *Escherichia coli* Ribonucleotide Reductase. *Biochemistry 43*, 5953−5964.
(77) Saleh, L., Kelch, B. A., Pathickal, B. A., Baldwin, J., Ley, B. A., and Bollinger, J. M. (2004) Mediation by Indole Analogues of Electron Transfer during Oxygen Activation in Variants of *Escherichia coli* Ribonucleotide Reductase R2 Lacking the Electron-Shuttling Tryptophan 48. *Biochemistry 43*, 5943−5952.
(78) Grzyska, P. K., Müller, T. A., Campbell, M. G., and Hausinger, R. P. (2007) Metal ligand substitution and evidence for quinone formation in taurine/α-ketoglutarate dioxygenase. *J. Inorg. Biochem. 101*, 797−808.

(79) Vojtechovský, J., Chu, K., Berendzen, J., Sweet, R. M., and Schlichting, I. (1999) Crystal Structures of Myoglobin-Ligand Complexes at Near-Atomic Resolution. *Biophys. J. 77*, 2153−2174.
(80) Mukherjee, A., Cranswick, M. A., Chakrabarti, M., Paine, T. K., Fujisawa, K., Münck, E., and Que, L. (2010) Oxygen Activation at Mononuclear Nonheme Iron Centers: A Superoxo Perspective. *Inorg. Chem. 49*, 3618−3628.
(81) Roelfes, G., Vrajmasu, V., Chen, K., Ho, R. Y. N., Rohde, J.-U., Zondervan, C., la Crois, R. M., Schudde, E. P., Lutz, M., Spek, A. L., Hage, R., Feringa, B. L., Münck, E., and Que, L. (2003) End-On and Side-On Peroxo Derivatives of Non-Heme Iron Complexes with Pentadentate Ligands: Models for Putative Intermediates in Biological Iron/Dioxygen Chemistry. *Inorg. Chem. 42*, 2639−2653.
(82) van der Donk, W. A., Krebs, C., and Bollinger, J. M. Jr. (2010) Substrate activation by iron superoxo intermediates. *Curr. Opin. Struct. Biol. 20*, 673−683.